

NUMERICAL APPROACH TO HIGH-THROUGHPUT OF NANOFIBERS BY A MODIFIED BUBBLE-ELECTROSPINNING

by

Jing YIN, Yi WANG, and Lan XU*

National Engineering Laboratory for Modern Silk, College of Textile and Clothing Engineering,
Soochow University, Suzhou, China

Original scientific paper
<https://doi.org/10.2298/TSCI2004367Y>

Nanofibers were prepared in large quantities using a modified bubble-electrospinning, where the distribution of electric field played an important role, and its distribution was studied numerically using 3-D Maxwell equation and verified experimentally. The results showed the increase of electric field strength could decrease the nanofiber diameter and enhance the nanofiber production.

Key words: *bubble-electrospinning, nanofiber alignment, positively charged ring, theoretical model*

Introduction

Electrospinning is a common method for preparing nanofiber membranes, which have a large specific surface area and very high porosity [1-10]. Its structure, size and morphology can be controlled, resulting in the applications in many fields, *e. g.*, nonwoven fabrics [11], reinforcing fibers [12], drug delivery systems [13], tissue engineering [14], filter materials [15], electrode materials [16], and so on.

Conventional electrospinning used a single-needle spinning, which limited its wide range of practical applications due to its low production. Recently, many improvements to the electrospinning technology have been made to enhance its output. Ding *et al.* [17] presented a multi-needle electrospinning system. Theron *et al.* [18] used a thin-walled circular foam tube to achieve multi-jet electrospinning. He *et al.* [19] invented the bubble-electrospinning (BE) technology which used an air pump to generate bubbles on the solution surface to generate jets, and the BE has been applied as an efficient free surface electrospinning for mass fabrication of nanofibers [20-22]. Shao *et al.* [20] proposed a modified bubble-electrospinning (MBE) using a conical air nozzle combined with a copper solution reservoir to improve the production of high-quality polyacrylonitrile (PAN) nanofibers. Fang *et al.* [21] applied the MBE apparatus to obtain high-throughput SF nanofibers. Yu *et al.* [22] combined the MBE set-up with a high speed rotating copper wire drum as a collector to produce high-throughput aligned nanofibers.

In this paper, PAN nanofibers have been prepared in large quantities using the MBE device presented in our previous work [20-22]. The schematic presentation of the MBE device is illustrated in fig. 1. In the MBE process, the distribution of electric field plays an important role [20]. The theoretical analyses and experimental researches were carried out to

* Corresponding author, e-mail: xlanmail@21cn.com

study the mechanism of the MBE, and the distribution of electric field was simulated by using Maxwell 3-D software. By comparing with the experimental data, the rationality of theoretical analysis was indicated. The results showed the increase of electric field intensity could decrease the nanofibers diameter, improve the diameter distribution and enhance the nanofiber production.

Theoretical analysis

When the electric field force is generated by the applied voltage, which would make the copper pipe charged positively to exceed the surface tension of the solution, numerous jets would be produced from the solution surface [23]. Figure 2 showed the forces at the point *a* of the jet when one of the jets emerged from the solution surface in the MBE process.

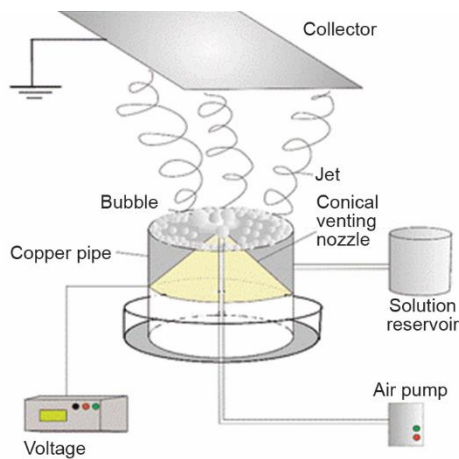


Figure 1. Schematic of the MBE apparatus

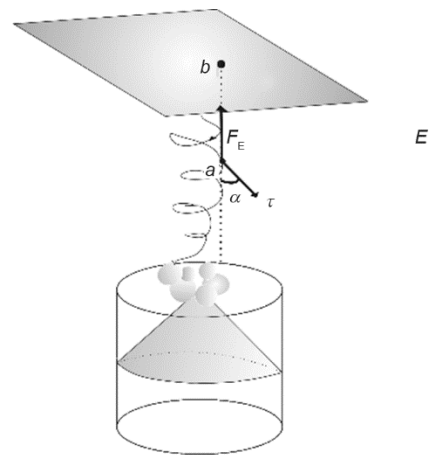


Figure 2. The forces at the point *a* of the jet in the MBE process

A centripetal force, resulting in the shrinking of the radius of whipping circle, was produced by the horizontal component of viscous force $\tau \sin \alpha$ during the spinning process. We assumed the vertical component of viscous force $\tau \cos \alpha$ contributes no work for the downward movement of the jet. Then the electric field force, F_E , would provide the kinetic energy of the moving jet and the upward movement of the jet would be generated:

$$\tau = av + bv^2 \quad (1)$$

$$F_E = q_a E \quad (2)$$

where v is the velocity of the jet, a and b – the constants to be further determined theoretically or experimentally, q_a – the signed magnitude of the point a charge, and E – the electric field intensity:

$$E = \frac{U}{d} \quad (3)$$

where U is the voltage applied by the high voltage power supply, and d – the distance from the solution surface to the collector.

Substituting eq. (3) into eq. (1), then F_E could be written in the following form:

$$F_E = q_a \frac{U}{d} \quad (4)$$

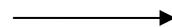
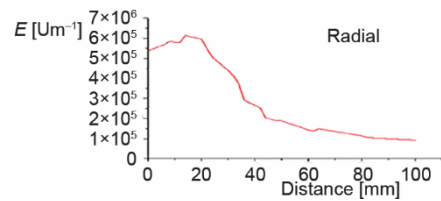
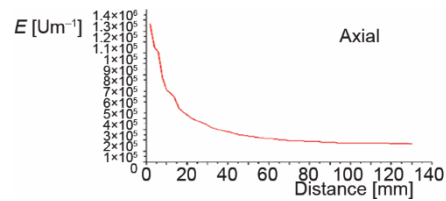
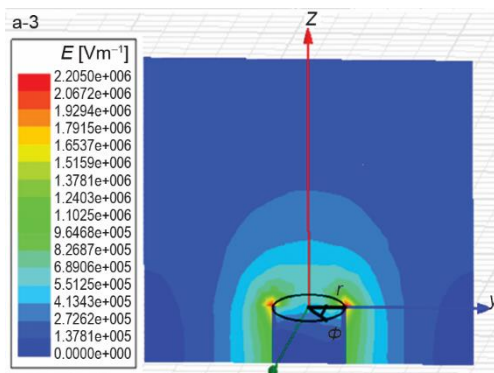
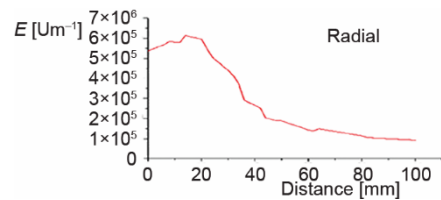
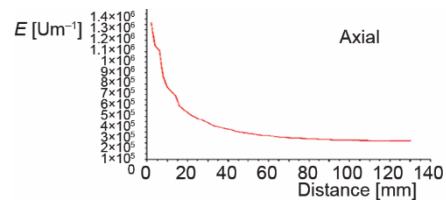
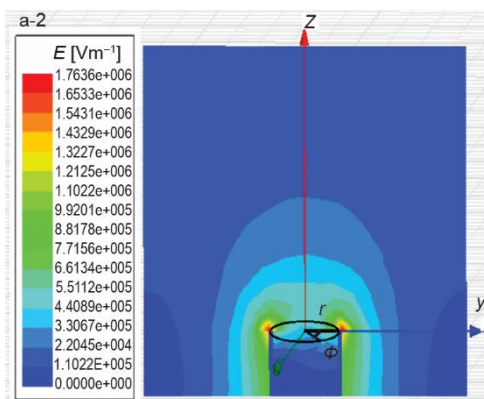
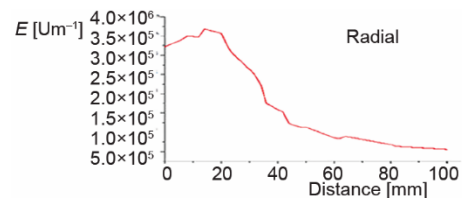
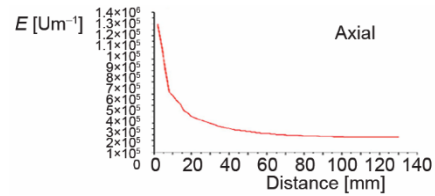
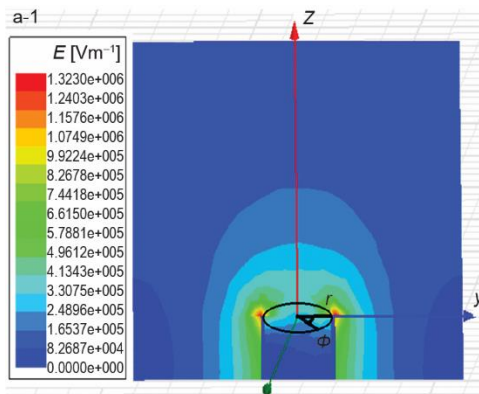
In view of eq. (4), the upward movement of the jet would be accelerated with the increase of the applied voltage, U , leading to an increase of the jet velocity. Therefore, the horizontal component of the viscous force would also increase according to eq. (1), which would result in the stability conditions. The diameter of the jet decreased with the increase of the jet velocity according to the conservation of mass [24, 25], causing the decrease of the electrospun nanofiber diameter. That means the electrospun nanofiber diameter would decrease as the applied voltage increased.

Simulation of electric field distribution

The variational-based finite element method are widely used in numerical methods, however, the present problem is complex and we have difficulty in establishing a needed variational formulation by the semi-inverse method [26-28], so a software is adopted for this purpose. In order to illustrate the aforementioned theoretical analysis results, the electric field distributions from the solution reservoir to the collector under the different applied voltages were simulated by Maxwell 3-D. The electric field simulations in the MBE process were carried out using the following parameters: the copper reservoir as positive electrode was a cylinder with a diameter of 40 mm and a height of 30 mm, the electric conductivity of copper was $5.8 \cdot 10^6$ simens/m, the working distance was 130 mm, the surface tension of PAN solution was 45 mN/m, the electric conductivity of the solution were 8.8 us/cm and the applied voltage varied from 30 kV to 70 kV. In addition, an electric field simulation of a conventional BE process at a voltage of 30 kV was performed and the solution reservoir made of polyethylene was a cylinder with the same size as that of the MBE. A conductive copper wire with a diameter of 2 mm, as the positive electrode, was inserted in the middle of the polymer reservoir and the tip of the copper wire was 5 mm below solution surface.

Figure 3 showed the simulation results of electric field distributions in the BE and MBE processes with different applied voltages. The figures on right were according to electric field distributions on the axial and radial directions of the reservoir top. In addition, the electric field strengths on the axial and radial directions of the reservoir top edge under the different applied voltages were indicated in fig. 4.

It could be seen from fig. 3(a) that the electric field strength at the top edge of the copper reservoir was maximum and made the top edge to produce jets more easily. Firstly, The electric field strength along the radial direction increased, then decreased as the distance from the top edge increased and finally stabilized. Meanwhile, the electric field strength along the axial direction gradually decreased. Figure 3(b) showed only the vicinity of the copper wire had a very strong electric field strength, causing the lower applied voltage. The electric field strength decreased rapidly along the axial and radial directions as the distance from the copper wire increased, and the electric field strength was rapidly reduced to zero in the range of 20 mm. As it is known, the electric field force is the major force to produce jets and the solution surface with higher electric field strength jets emerge more easily [20]. Therefore, the MBE could emerge more jets under a much higher applied voltage which would improve the production of nanofibers compared with the BE. And the solution surface near the top edge of the copper reservoir was most prone to generate many jets. As shown in fig. 4, the higher the applied voltage, the greater the electric field along the axial and radial directions. And the simulation results were in agreement with the previous theoretical analysis.



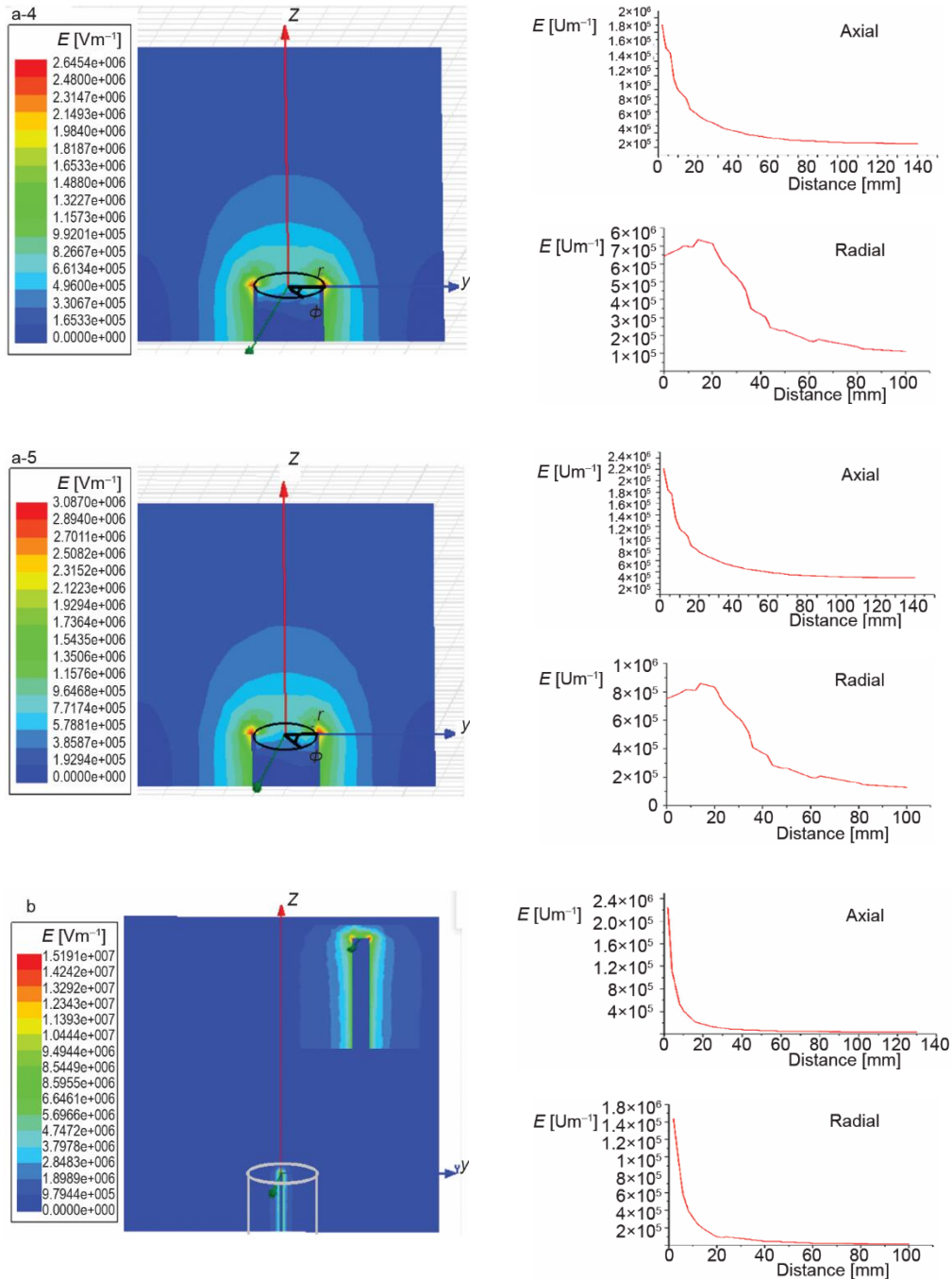


Figure 3. Simulations of the electric field distributions, (a) MBE with different applied voltage (a-1: 30 kV; a-2: 40 kV; a-3: 50 kV; a-4: 60 kV; a-5: 70 kV); (b) BE (30 kV), Inset: Local magnification; the right figures were the according to electric field intensities on the axial and radial directions of the reservoir top

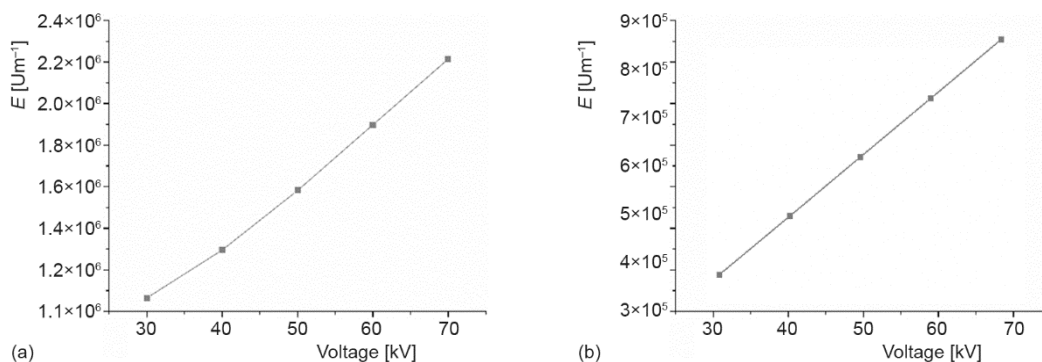


Figure 4. The electric field strengths on the axial and radial directions of the reservoir top edge under the different applied voltages; (a) axial direction (b) radial direction

Experimental verification

The PVA with $1750^\circ \pm 50^\circ$ of polymerization was dissolved in deionized water to obtain PVA aqueous solution of 7 wt.% concentration. Then the solution was stirred at 60°C for 4 hours in water until it became homogeneous. In the MBE process, the spinning parameters were: the collecting distance from the solution surface to the collector was 130 mm and the applied voltage varied from 30 to 70 kV. The PVA solution was poured into the reservoir,

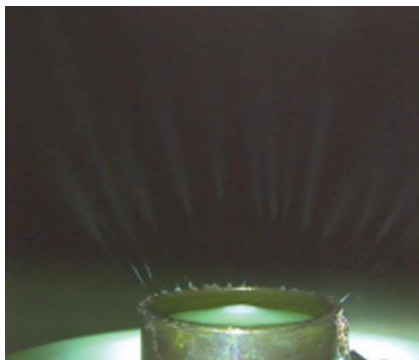


Figure 5. Photograph of the MBE process [20]

then the gas valve was turned on slowly and multiple jets initiated at the solution surface after voltage was applied, see fig. 5. It could be observed that more jets emerged from the solution surface near the top edge of the copper reservoir and the phenomena were consistent with the previous simulation results.

The morphologies of PVA nanofibers produced by MBE and BE under the different applied voltages were shown respectively in fig. 6. The average diameters and the production of PVA nanofibers obtained were illustrated in tab. 1. The SEM images of nanofibers obtained by MBE with different applied voltages were indicated in fig. 6(a1-a5) and those of BE were illustrated in fig. 6(b). The results showed the average diameter of nanofibers prepared by MBE was smaller than that of BE at the same applied voltage (30

kV) and the production of nanofibers obtained by MBE was higher than that of BE. In addition, as the applied voltage increased in MBE process, the average diameter of nanofibers decreased firstly and then increased and the production of nanofibers increased, as shown in tab. 1. This was because too highly accelerated upward movement of the jet would not further stretch the jet into smaller fibers when the applied voltage was too high [20]. The experimental data were in accordance with the simulation and theoretical analysis results and illustrated the average diameter of electrospun nanofibers decreased and the production of those increased as the applied voltage increased.

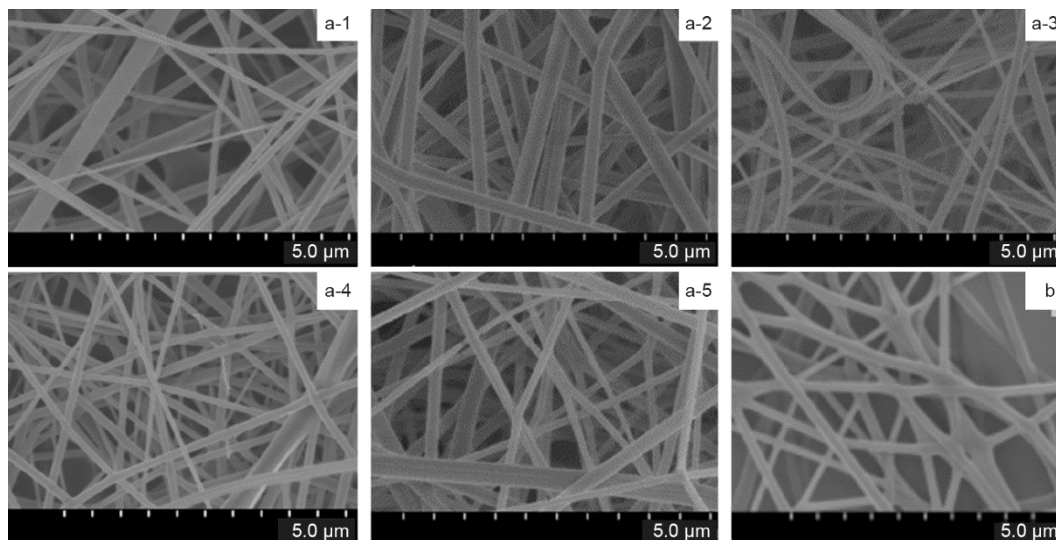


Figure 6. The SEM images of PVA nanofibers, (a) MFSE with different applied voltage (a-1 30 kV, a-2 40 kV, a-3 50 kV, a-4 60 kV, a-5 70 kV); (b) BE (30 kV) [20]

Table 1. Average diameter and production of PVA nanofibers produced by MBE and BE, respectively, under the different applied voltages [20]

Spinning method	Applied voltage [kV]	Average diameter [nm]	Production [gh ⁻¹]
MBE	30	136 ± 8.53	3.5
MBE	40	151 ± 9.26	14.4
MBE	50	132 ± 7.89	19.8
MBE	60	108 ± 7.63	45
MBE	70	142 ± 8.48	72
BE	30	190 ± 8.26	3

Conclusion

In this paper, nanofibers have been fabricated in large quantities using a MBE with a copper solution reservoir. The mechanism of the MBE was studied by simulating the distribution of electric field using Maxwell 3-D and theoretical analysis which was verified by the experiment data. The experimental data were in accordance with the simulation and theoretical analysis results. The results showed the electric field distribution of the MBE was more uniform than that of the BE and the MBE could produce more jets under a much higher applied voltage which would improve the production of nanofibers. Meanwhile, more jets emerged from the solution surface near the top edge of the copper reservoir in the MBE process. Therefore, the increase of the applied voltage could decrease the nanofiber diameter and enhance the nanofiber production in the MBE process.

Acknowledgment

The work is supported financially by National Natural Science Foundation of China (Grant No. 11672198), PAPD (A Project Funded by the Priority Academic Program Devel-

opment of Jiangsu Higher Education Institutions), and Six Talent Peaks Project of Jiangsu Province (Grant No. GDZB-050).

References

- [1] Tian, D., *et al.*, Geometrical Potential and Nanofiber Membrane's Highly Selective Adsorption Property, *Adsorption Science & Technology*, 37 (2019), 5-6, pp. 367-388
- [2] Li, X. X., *et al.*, Nanoscale Adhesion and Attachment Oscillation Under the Geometric Potential, Part 1: The Formation Mechanism of Nanofiber Membrane in the Electrospinning, *Results in Physics*, 12 (2019), Mar., pp. 1405-1410
- [3] He, J. H., *et al.*, Review on Fiber Morphology Obtained by Bubble Electrospinning and Blown Bubble Spinning, *Thermal Science*, 16 (2012), 5, pp. 1263-1279
- [4] Liu, Z., *et al.*, Active Generation of Multiple Jets for Producing Nanofibres with High Quality and High Throughput, *Materials & Design*, 94 (2016), Mar., pp. 496-501
- [5] Liu, Z., *et al.*, Tunable Surface Morphology of Electrospun PMMA Fiber Using Binary Solvent, *Applied Surface Science*, 364 (2016), Feb., pp. 516-521
- [6] Liu, Z., *et al.*, Needle-Disk Electrospinning Inspired by Natural Point Discharge, *Journal of Materials Science*, 52 (2017), 4, pp. 1823-1830
- [7] Li, Y., He, J. H., Fabrication and Characterization of ZrO₂ Nanofibers by Critical Bubble Electrospinning for High-Temperature-Resistant Adsorption and Separation, *Adsorption Science & Technology*, 37 (2019), 5-6, pp. 425-437
- [8] Zhou, C. J., *et al.*, Silkworm-Based Silk Fibers by Electrospinning, *Results in Physics*, 15 (2019), Dec., 102646
- [9] Chen, R. X., *et al.*, Numerical Approach to Controlling a Moving Jet's Vibration in an Electrospinning System: An Auxiliary Electrode and Uniform Electric Field, *Journal of Low Frequency Noise, Vibration and Active Control*, 38 (2019), 3-4, pp. 1687-1698
- [10] Zhao, J. H., *et al.*, Needle's Vibration in Needle-Disk Electrospinning Process: Theoretical Model and Experimental Verification, *Journal of Low Frequency Noise, Vibration and Active Control*, 38 (2019) 3-4, pp. 1338-1344
- [11] Kishimoto, Y., *et al.*, Comparisons between Silk Fibroin Nonwoven Electrospun Fabrics Using Aqueous and Formic Acid Solutions, *International Journal of Polymeric Materials and Polymeric Biomaterials*, 67 (2018), Mar., pp. 462-467
- [12] Song, Y. H., *et al.*, Preparation and Characterization of Highly Aligned Carbon Nanotubes/Polyacrylonitrile Composite Nanofibers, *Polymers*, 9 (2017), 1, ID 1
- [13] Liu, X. K., *et al.*, Tunable Zero-Order Drug Delivery Systems Created by Modified Triaxial Electrospinning, *Chemical Engineering Journal*, 356 (2018), Jan., pp. 886-894
- [14] Mehra, M., *et al.*, Electrospun Aligned PLGA and PLGA/Gelatin Nanofibers Embedded with Silica Nanoparticles for Tissue Engineering, *International Journal of Biological Macromolecules*, 79 (2015), 9, pp. 687-695
- [15] Kadam, V.V., *et al.*, Electrospun Nanofibre Materials to Filter Air Pollutants – A review, *Journal of Industrial Textiles*, 47 (2018), 8, pp. 2253-2280
- [16] Armer, C. F., *et al.*, Electrospun Vanadium-Based Oxides as Electrode Materials, *Journal of Power Sources*, 395 (2018), Aug., pp. 414-429
- [17] Ding, B., *et al.*, Fabrication of Blend Biodegradable Nanofibrous Nonwoven Mats Via Multi-Jet Electrospinning, *Polymer*, 45 (2004), 6, pp. 1895-1902
- [18] Theron, S. A., *et al.*, Multiple Jets in Electrospinning: Experiment and Modeling, *Polymer*, 46 (2005), 9, pp. 2889 -2899
- [19] He, J. H., *et al.*, Biomimic Fabrication of Electrospun Nanofibers with High-Throughput, *Chaos Solitons & Fractals*, 37 (2008), 3, pp. 643-651
- [20] Shao, Z. B., *et al.*, High-Throughput Fabrication of Quality Nanofibers Using a Modified Free Surface Electrospinning, *Nanoscale Research Letters*, 12 (2017), 1, ID 470
- [21] Fang, Y., *et al.*, High-Throughput Preparation of Silk Fibroin Nanofibers by Modified Bubble-Electrospinning, *Nanomaterials*, 8 (2018), 7, ID 471
- [22] Yu, L., *et al.*, High Throughput Preparation of Aligned Nanofibers Using an Improved Bubble-electrospinning, *Polymers*, 9 (2017), 12, ID 658

- [23] Shao, Z. B., *et al.*, Formation Mechanism of Highly Aligned Nanofibers by a Modified Bubble-Electrospinning, *Thermal Science*, 22 (2018), 1A, pp. 5-10
- [24] Tang, X. P., *et al.*, Effect of Flow Rate on Diameter of Electrospun Nanoporous Fibers, *Thermal Science*, 18 (2014), 5, pp. 1439-1441
- [25] Zhao, J. H., *et al.*, Experimental and Theoretical Study on the Electrospinning Nanoporous Fibers Process, *Materials Chemistry and Physics*, 170 (2016), 6, pp. 294-302
- [26] He, J. H. A Modified Li-He's Variational Principle For Plasma, *International Journal of Numerical Methods for Heat and Fluid Flow*, On-line first, <https://doi.org/10.1108/HFF-06-2019-0523>, 2019
- [27] He, J. H. Lagrange Crisis and Generalized Variational Principle for 3-D unsteady flow, *International Journal of Numerical Methods for Heat and Fluid Flow*, On-line first, <https://doi.org/10.1108/HFF-07-2019-0577>, 2019
- [28] He, J. H., Sun, C., A Variational Principle for a thin Film Equation, *Journal of Mathematical Chemistry*. 57(2019), 9, pp. 2075-2081